

# Early Studies of a New Transmission Mechanism for Manipulator Actuation Designed for MR-guided Interventions

Haoran Zhao, Xin Liu, Habib M. Zaid, Dipan J. Shah,  
Michael J. Heffernan, Aaron T. Becker, and Nikolaos V. Tsekos

**Abstract**—Magnetic resonance imaging (MRI)-guided, manipulator-assisted interventions have the potential to improve patient outcomes. This work presents a force transmission mechanism, called solid-media transmission (SMT), for actuating manipulators inside MRI scanners. The SMT mechanism is based on conduits filled with spheres and spacers made of a nonmagnetic, nonconductive material that forms a backbone for bidirectional transmission. Early modeling and experimental studies assessed SMT and identified limitations and improvements. Simulations demonstrated the detrimental role of friction, that can be alleviated with choice of low friction material and long spacers limited by the desired bending of the conduit.

A closed-loop control law was implemented to drive the SMT. The 3rd order system fit ratio is 92.3%. A 1-m long SMT was experimentally tested under this closed-loop controller with heuristically set parameters using a customized benchtop setup. For commanded displacements of 1 to 50 mm, the SMT-actuated 1 degree of freedom stage exhibited sub-millimeter accuracy, which ranged from  $0.109 \pm 0.057$  mm to  $0.045 \pm 0.029$  mm depending on the commanded displacement. However, such accuracy required long control times inversely proportional to displacement ranging from  $7.56 \pm 1.85$  s to  $2.53 \pm 0.11$  s. This was attributed to friction as well as backlash which is due to suboptimal packing of the media. In MR studies, a 4-m long SMT-actuated 1 DoF manipulator was powered by a servo motor located inside the scanner room but outside the 5 Gauss line of the magnet. With shielding and filtering, the SNR of MR images during the operation of the servo motor and SMT-actuation was found to be  $89 \pm 9\%$  of the control case.

## I. INTRODUCTION

Magnetic resonance imaging (MRI) is a powerful diagnostic modality that is well established in pre-operative planning of interventions and surgeries. MRI is also advocated and emerging for real-time intra-operative guidance because it has excellent soft tissue contrast, lack of ionizing radiation, and an internal coordinate system to co-register on-the-fly tools and images. To address the limited access to patients inside the high magnetic field cylindrical clinical MRI scanners, and advance intra-operative MRI, MR-compatible robotic manipulators have been proposed to telerobotically maneuver interventional tools, such as biopsy or ablation needles [1]–[5]. These manipulators must: (a) fit and operate inside the limited space of a high-field MR scanner (60–70 cm cylinder) together with the patient; (b) operate in

H. Zhao and A. Becker are with the Dept. of Electrical and Computer Engineering, X. Liu, H.M. Zaid and N.V. Tsekos are with the Medical Robotics Lab, Dept. of Computer science, University of Houston, Houston, TX 77004, USA, D. Shah is with the Cardiovascular MRI Laboratory, Houston Methodist DeBakey Heart & Vascular Center, M.J. Heffernan is with GuidaBot, LLC. hzhao9@uh.edu, atbecker@uh.edu, nvtsekos@Central.uh.edu.

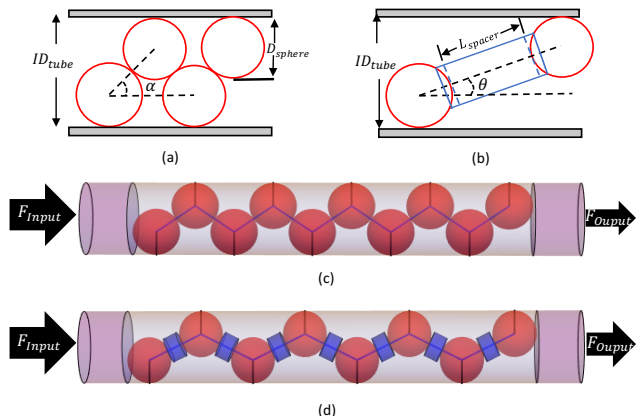


Fig. 1. (a) Illustration of SMT sphere packing. (b) Illustration of SMT spacer and sphere packing. (c) Sphere zigzag packing model. (d) Sphere and spacer zigzag packing model. In the actual backbone, the spacers are hollow and the spheres fit partly inside.

the presence of up to 3 Tesla magnetic fields and rapidly switching magnetic field gradients (200 mT/m/ms and peak strength 40 mT/m); (c) be safe; (d) not induce imaging artifacts, for example, secondary to magnetic susceptibility, distortion of the linearity gradients, or generation of electromagnetic interference (EMI). Among the critical technologies to enable MR-compatible telemanipulation is suitable force transmission mechanisms.

The limited space inside the cylindrical scanners causes most MR manipulators to place the power units outside the gantry and, thus, away from the isocenter of the scanner where the manipulator resides by the patient. Then a transmission is used to link the powering unit and the manipulator, such as mechanical drives [6]–[9] and fluidic systems [10]–[16]. Mechanical drives offered improved kinematic performance and are used successfully for both general purpose and anatomy-specific applications. Ultrasonic motors (USM) that are commonly used, can be produced without magnetic material, offer excellent resolution, have rotary or linear motor form, and have powerless braking. Fluidic transmissions have been extensively studied for MR compatible manipulation, including pneumatic [11]–[15] and hydraulic [15], [16] systems. They offer flexible routing and can be made nonmagnetic and nonconductive. Notable is the PneuStep, a pioneering pneumatic stepper motor developed for MR manipulators [17]. While these and other works have

advanced the field of MR manipulation, each actuation form exhibits benefits and limitations. For example, mechanical drives require rigid frame structures and fixed transmission routing. This may be appropriate for access to the prostate [10], the breast [7], or the brain [8]; however, flexible routing is preferred and may be necessary for logistics and ergonomics in patient setup and access, and non-obstructing arrangements in the MR scanner room. The robot is usually placed at the scanner's isocenter. Due to motor size and EMI, USM are usually placed at a distance from the scanner, requiring structural provisions and mechanical linkages, as we have done before [7], [18]. EMI from USM can cause as high as 40%-60% reduction in SNR [6], [9], [10], [19]–[21], requiring interleaving imaging and actuation [19], filtered drivers [20], and shielding [9], [21]. Fluidic actuators are complicated, expensive, and require MR-compatible valves, cylinders, and pistons; otherwise, the piston-powering motors must be placed outside the room to avoid EMI [6], [17], [20], [22]. Also, MR manipulation comparison study has shown that direct-drive actuators exhibit better kinematic performance [22].

As major groundbreaking efforts, including the above works, have enabled and advanced the field of MR-compatible manipulators, exploring new actuation and kinematic structures is an on-going effort due to the potential clinical impact. Within this context, we proposed an alternative mechanism, called solid media transmission (SMT), that resembles fluidic actuators but its conduits are filled with solid media in the form of spheres interleaved with spacers as shown in Fig. 1. Pilot proof of concept studies illustrated the feasibility of MR compatible SMT actuation with open-loop control [23], as well as introduced SMT-based force amplifiers and multi-port manifolds [24].

As SMT is a new mechanism, the purpose of this work was to investigate some of the fundamental aspects of this uncharted territory. In these studies, we first implemented a model for the SMT mechanism and then assessed the role of the most obvious aspects: friction, dimensions of componentry, and media packing. Benchtop experimental studies were then focused on assessing a preliminary version of a closed-loop control of the SMT that demonstrated the ability for sub-millimeter accuracy, as well as the challenge of achieving consistent media packing. Finally, MR experimental studies with a one degree-of-freedom (DoF) SMT-actuated manipulator assessed the MR compatibility of the mechanism as well as the potential for using conventional electromagnetic motors inside the MR scanner room. The paper is organized as follows: In Section II, we describe the theoretical basis of the SMT mechanism. Section III presents (i) the experiment setup and studies and positioning performance of closed-loop control with a proportional-integral-derivative controller (PID) with time delay, and (ii) results from MR compatibility studies of a one DoF SMT-actuated manipulator at a 1.5 Tesla Scanner. Finally, we discuss the findings of these studies in Section IV and outline future work in Section V. Table 1 reviews the findings and conclusions of this work.

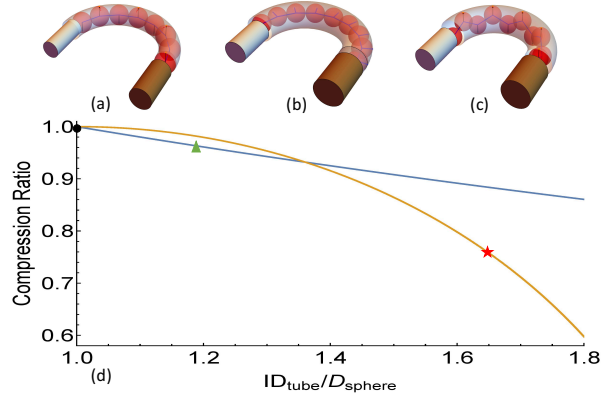


Fig. 2. Compression ratios for tubing bend diameter  $D_{\text{bend}} = 5D_{\text{sphere}}$ : (a) Compression ratio for  $ID_{\text{tube}} = D_{\text{sphere}}$  shown with a black dot. (b) Compression ratio when spheres and spacers are pushed to outside wall shown with a green triangle. (c) Compression ratio for zigzag packing shown with a red star.

## II. SOLID MEDIA TRANSMISSION MECHANISM

### A. The SMT Backbone

The SMT mechanism is composed of a plurality of solid, discrete media packed inside a conduit. Fig. 1 illustrates how the solid media is employed in the work, i.e. spheres with a diameter of  $D_{\text{sphere}}$  and spacers with a length of  $L_{\text{spacer}}$  are inside a conduit with inner diameter  $ID_{\text{tube}}$ . When packed inside the conduit, they assume a zigzag pattern. Packing of SMT media occurs secondary to the application of a force to achieve the minimum compression ratio, i.e. the horizontal distance between two spheres divided by the sphere diameter. The media are arranged in this zigzag pattern, since the solid sphere diameter  $D_{\text{sphere}}$  should be less than inner tubing diameter  $ID_{\text{tube}}$  to ensure that the media can freely move inside the conduit. Moreover,  $ID_{\text{tube}}/D_{\text{sphere}}$  must be small enough to prevent the zigzag packing from collapsing on itself and generating multiple points of contact, this allowable ratio is:

$$\frac{ID_{\text{tube}}}{D_{\text{sphere}}} \in \left[ 1, 1 + \frac{\sqrt{3}}{2} \right) \quad (1)$$

The simplest SMT is filled with spheres and no spacers and can be actuated by extending a pushing rod outside the channel lumen through a slot. For sphere-only composition, when force is applied the spheres align in a zigzag pattern, where the angle  $\alpha$  between the axis of the channel and center to center of spheres, as shown in Fig. 1a is:

$$\alpha = \arcsin \left( \frac{ID_{\text{tube}} - D_{\text{sphere}}}{D_{\text{sphere}}} \right) \quad (2)$$

For SMT composed of spheres and spacers, the angle  $\theta$  between the axis of the channel and center to center of spheres, shown as Fig. 1b is:

$$\theta = \arcsin \left( \frac{ID_{\text{tube}} - D_{\text{sphere}}}{D_{\text{sphere}} + L_{\text{spacer}}} \right) \quad (3)$$

Spacers increase the efficiency of force transmission. Comparing equation (2) and (3) shows that lengthening the spacer reduces the angle between the axis of the channel and the center-to-center line of the sphere, which means spacers reduce the magnitude of forces orthogonal to the pushing direction, and increase the force transmitted along the central axis of the tubing.

For a variety of MR compatible actuated devices, the SMT line must be routed from the power source to the isocenter inside the scanner gantry and, thus, assume a curved posture. Packing arrangements are different in straight and bent tubing. When spheres with cylindrical spacers are used and they pass through a curve, there is an additional important geometric feature to be considered to avoid a spacer binding or colliding with the conduit wall. The bending radius ( $D_{\text{bend}}/2$ ) of a given conduit with diameter  $ID_{\text{tube}}$  and the length ( $L_{\text{spacer}}$ ) of spacer, determines the maximum diameter ( $D_{\text{spacer}}$ ) of the spacer:

$$D_{\text{spacer}} \in \left[ 0, \cos \left( \arcsin \left( \frac{L_{\text{spacer}} + D_{\text{sphere}}}{D_{\text{bend}} + ID_{\text{tube}} - D_{\text{sphere}}} \right) \right) (D_{\text{bend}} + ID_{\text{tube}} - D_{\text{sphere}}) - (D_{\text{bend}} - ID_{\text{tube}}) \right] \quad (4)$$

Inside a bend, the SMT backbone arranges itself to minimize the compression ratio. As illustrated in Fig. 2, in a bend the spheres are either all are pushed against the outer wall of the tube (Fig. 2b) or are in a pattern that zigzags parallel to the axis of curvature along the tube centerline (Fig. 2c). If the spheres are centered in the tube, the angle advanced along the bend from one sphere to the next is:

$$\beta = \arccos \left( 1 - \frac{D_{\text{sphere}}^2}{D_{\text{bend}}} \right) \quad (5)$$

When the spheres are all are pushed against the outer wall of the tubing, the angle advanced along the bend from one sphere to the next is:

$$\gamma = \arccos \left( 1 - \frac{2D_{\text{sphere}}^2}{(D_{\text{tube}} - D_{\text{sphere}} + D_{\text{bend}})^2} \right) \quad (6)$$

and the compression ratio is:

$$\eta_1 = \frac{\gamma}{\beta} \quad (7)$$

For the zigzag pattern, the angle advanced along the bend from one sphere to the next is:

$$\delta = \arccos \left( \frac{D_{\text{bend}}^2 + 2(D_{\text{tube}} - 4)D_{\text{tube}}}{2D_{\text{bend}}^2} \right) \quad (8)$$

and the compression ratio is:

$$\eta_2 = \frac{\delta}{\beta} \quad (9)$$

For low ratios of  $\frac{ID_{\text{tube}}}{D_{\text{sphere}}}$  the spheres are pushed to the outside of the bend, and for high ratios the spheres assume a zigzag pattern. The switch occurs when  $\eta_1$  equals  $\eta_2$ .

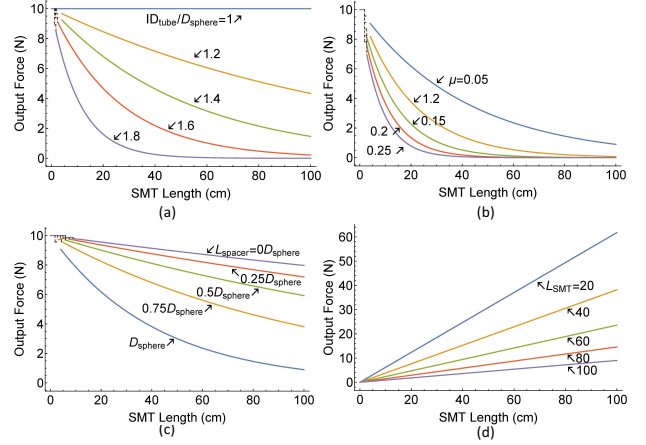


Fig. 3. Parameter study: (a) different SMT line lengths, (b) different friction coefficients, (c) different ratio of  $ID_{\text{tube}}$  and  $D_{\text{sphere}}$ , (d) different spacer lengths. Simulation performed in Mathematica, code available at [25].

### B. Friction in the SMT mechanism

Friction exists in all mechanical systems, e.g. bearings, fluidic system cylinders, and transmissions, and appears at the physical interface between any two surfaces in relative movement. In the SMT system, friction is the main cause of system delay and reduction in the force transmission efficiency. As shown before in [24], [26], when the mass of a sphere or spacer component is small compared to the input force, output force, or friction, we can neglect the effect of gravity. Moreover, for the particular SMT mechanism studied in this work (i.e. dimensions and materials), experimental observations confirm that the spheres slide without rolling. Therefore, our model considers sliding spheres but not rolling spheres. Due to the complexity of analyzing an entire SMT backbone and based on prior work [27], we decompose the SMT backbone to each individual sphere and then model the friction of entire backbone with a piecewise function.

For a two-sphere backbone ( $N_{\text{sphere}} = 2$ ), the center to center distance  $Z$  of the two spheres is:

$$Z = \sqrt{2D_{\text{sphere}}(L_{\text{spacer}} + ID_{\text{tube}}) + L_{\text{spacer}}^2 - ID_{\text{tube}}^2} \quad (10)$$

Therefore the relationship between input force and output force is:

$$F_{\text{Out}} = F_{\text{In}} \left( 1 - 2\mu \frac{ID_{\text{tube}} - D_{\text{sphere}}}{Z} \right) \quad (11)$$

where  $\mu$  is the friction coefficient of the tubing materials. For a given length  $L_{\text{SMT}}$  of the SMT conduit (which is a parameter used in prototyping a system), the number of spheres  $N_{\text{sphere}} > 2$  needed to form a packed backbone is:

$$N_{\text{sphere}} = \frac{L_{\text{SMT}}}{Z} \quad (12)$$

At this case, after assigning  $c$  equal to the right hand of equation (9) for clarity, output force is:

$$F_{\text{Out}} = c \left( 1 - \mu \frac{ID_{\text{tube}} - D_{\text{sphere}}}{Z} \right)^{N_{\text{sphere}} - 2} \quad (13)$$

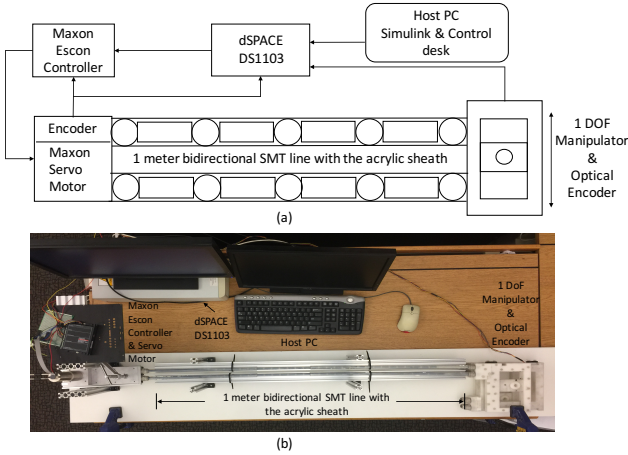


Fig. 4. The experimental setup for control studies: (a) block diagram of each component and connections, (b) photograph of customized experimental setup

Fig. 3 presents simulation results highlighting certain features of the SMT mechanism. As shown in Fig. 3a and intuitively expected, the friction of the entire SMT backbone increases with increased length of the tubing (i.e. the  $N_{\text{sphere}}$ ). To reduce friction, the tubing should be as short as possible, but must achieve the goal of transmission distance. As underscored in Fig. 3b to d, solutions to improve force transmission efficiency include any or a combination of the following: selecting componentry material with lower friction coefficient, decreasing the  $ID_{\text{tube}}$  of the conduit, or increasing the length of the spacer. The top row in Table 1 reviews the modeling findings.

### III. EXPERIMENT STUDIES

#### A. Experimental Set-Up

To further understand the SMT mechanism, we implemented the customized experimental setup shown in Fig. 4. We used a PC-based real-time controller (Advanced control Education Kit1103, dSPACE Inc Wixom, MI). Based on the velocity and displacement requested by the operator, the dSPACE controller calculated a corresponding pulse-width modulation (PWM), directional signal, and enabling signal. These signals controlled a Maxon Escon amplifier (DES 50/5, digital 4-Q-EC Servoamplifier 50 V / 5 A, USA subsidiary) that was driving a Maxon servo motor (Motor - DCX35L GB KL 24V). The servo was powering a 43:1 rack and pinion that actuated two opposite-movement rods for bidirectional actuation of a 1-meter long SMT line. The SMT lines were then connected to a stage of the manipulator that had an optical encoder to record displacement; the signal of the optical encoder was sampled by the dSPACE controller. The experiment control and measurement code was programmed in Simulink, the real-time control code was automatically generated and then downloaded to the PPC750GX and TMS320F240 DSP located on the DS1103 board for the drive motor and data acquisition, respectively.

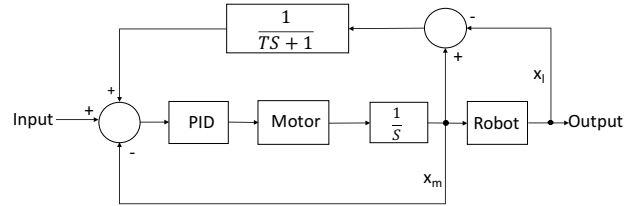


Fig. 5. Block diagram of PID closed-loop control with time delay

To monitor and track experimental data in real-time, we used control desk (dSPACE GmbH, US subsidiary).

For closed-loop control experiments, we used 1 meter long nylon tubing with an  $ID = 7\text{mm}$  and an  $OD = 9\text{mm}$ , filled with  $D_{\text{sphere}} = 6.23\text{mm}$  nylon spheres and nylon spacers with  $L_{\text{spacer}} = 20\text{mm}$ . Experimental data were captured and plotted in real time with 1kHz sample rate. The nylon tubing was inserted into a UV-extruded Acrylic tube ( $OD = 15\text{mm}$ ,  $ID=9.35\text{mm}$ ). The external sheath was used to ensure the rigidity of the channel and prevent elastic deformation of nylon tubing when the motor applies force.

#### B. Closed-Loop SMT Control

Early open-loop studies demonstrated that this SMT setup exhibited displacement errors and response delays principally due to backlash originating from gaps between spheres and spacers [26]. When the gaps exist, the motor loses contact with the load, and the force generated by the motor only drives the motor itself (and parts of the force transmission, such as rods and shaft) and not the load. Controlling systems with backlash has been investigated since the 1940's. The deleterious effects of backlash include decreased steady state accuracy and degree of stability. Examples include robotic arms [28] and rolling mills [29], both proposed to control position and speed in the presence of backlash. To minimize backlash influence, we tested closed-loop control to achieve the goal. As analyzed in [30], feedback can be from the motor side, load side, or motor and the load side. In our design, we use feedback from both the motor's optical encoder and manipulator's optical encoder. The Maxon encoder feedback from the motor side is used for velocity control. The robot side feedback control is used for position accuracy control.

We used a PID controller with a feedback mechanism that continuously calculates an error value  $e(t)$  as the difference between the desired goal and measured value, and applies a correction based on the proportional (P), integral (I) and derivative (D) parts of:

$$u(t) = K_P e(t) + K_I \int_0^t e(\tau) d\tau + K_D \frac{de(t)}{dt} \quad (14)$$

Since backlash introduces phase lags that cause oscillations or instabilities, our controller was designed to imitate the modified dual loop PID controller described in [31] and

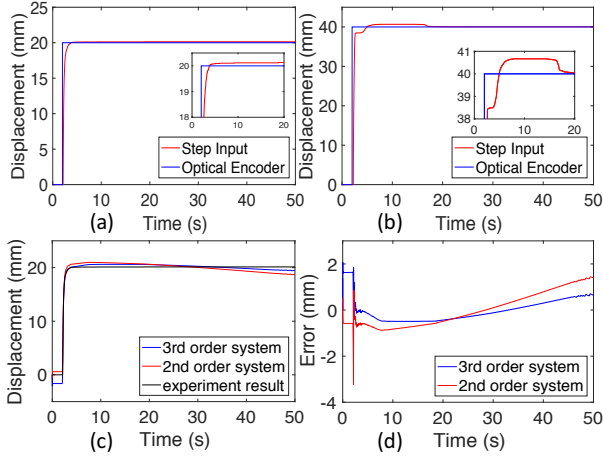


Fig. 6. (a) 20mm step input vs. experiment result (b) 40mm step input vs. experiment result (c) response to 20mm step input by experiment compared to 3<sup>rd</sup> order and 2<sup>nd</sup> order models (d) estimated system error compared with experiment result.

shown in Fig. 5. Feedback of motor and manipulator position contributes to controlling the system response. The motor position feedback ( $X_m$ ) is designed to meet the transient response. By passing the angular difference signal:

$$X_d = X_m - X_1 \quad (15)$$

The feedback in the steady state is equal to:

$$-X_m + \frac{1}{T_s + 1}(X_m - X_1) \quad (16)$$

If the time constant  $T = 0$ , the equation will be equal  $-X_1$ . As  $T$  tends to infinity, the result approaches  $-X_m$ .

From prior works [23] and [26], we consider that the SMT system has three key parameters: ratio  $ID_{\text{tube}}/D_{\text{sphere}}$ ,  $\mu$ , and the elasticity of conduit tubing. We lack an accurate finite element analysis (FEA) model of the SMT line. To determine the appropriate number of state variables, we use the MATLAB System Identification toolbox. The system identification toolbox estimated the continuous time transfer function using time domain data and state space, using the State Variable Filter (SVF) and Instrument Variable (IV) methods [32] and [33]. First, we compared the 20 mm step signal and 40 mm step signals (both step times start at 2 seconds and last 50 seconds). As shown in Fig. 6a and b, the 40 mm step signal resulted in a much higher overshoot than the 20 mm step. Overshoot might be caused by higher instant force input. The flat form of the overshoot might be caused by elastic deformation. MATLAB System Identification toolbox was also used to assess the order of the system. This study revealed that when the system is modeled as a 2<sup>nd</sup> order system, its fit ratio is 82.5%, while the fit ratio reaches 92.3% when modeled as a 3<sup>rd</sup> order system. This supports our initial assumption that the system has three dominant state variables.

Under proportional control, large magnitude step commands generate proportionally large input forces. This in-

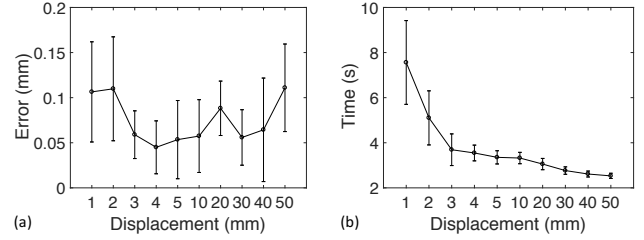


Fig. 7. Illustration of system characteristic with 1 to 5 mm and 10 to 50mm ramp input. Each data point is 10 trials. (a) shows the mean and deviation of system error, (b) shows the mean and deviation of system delay.

creases overshoot at the beginning because the DC motor has a maximum velocity and can not replicate an input step in position. To reduce the influence of overshoot response, we changed input signal from a step function to a ramp function to assess the error tolerance and response delay. The ramp function input was tested for 1, 2, 3, 4, 5 mm and 10, 20, 30, 40, 50 mm commanded displacement. Each set repeated 10 times with random direction. As shown in Fig. 7a, these studies demonstrated that the average displacement error was 0.075 mm with a standard deviation is 0.042 mm (total  $n=100$  measurements), This studies clearly demonstrate that 1-m long made of nylon SMT with the particular closed-loop controller can achieve a positioning accuracy of less than 0.1 mm. However, Fig. 7b clearly shows us that the response delay is long ranging from  $7.56 \pm 1.85$  s to  $2.53 \pm 0.11$  s. The average delay is 3.75 s, and the average deviation is about 0.53 s. An interesting result was that the delay was inversely correlated to the commanded displacement. The middle row of Table 1 reviews the findings of the experimental studies.

### C. MR Studies

MR studies to assess the compatibility of the SMT mechanism were performed on a 1.5 T scanner (Avanto, Siemens Healthcare), using the 1-DoF manipulator powered with 4-m long SMT lines (unlike the benchtop studies, these nylon tubing did not have an acrylic sheath). With this setup, inside the MR scanner room were the servo motor and an electronics box positioned sideways, i.e. orthogonal to the magnet axis, and outside the 5 Gauss line at 2.5 m away. The electronics box included regulated power supplies, motor controller, and filters, and was communicating with the Host PC outside the scanner room via an optical cable that entered the scanner room via the wall waveguide. To reduce EMI, based on our prior work [23] and [34]: (i) the electronics box was surrounded by a custom-made Faraday cage, (ii) the cable shield, from the controller to the servo motor, and the shield of the electronics box were grounded together to the scanner room ground, and (iii) a low pass filter was used for the drive signals. Three MR studies were performed using the body RF coil of the scanner for transmission and signal reception, homogenous phantoms, and a TrueFISP pulse sequence (TR = 3.2 ms; TE = 1.46 ms; Excitation Angle = 85°; matrix size = 192×192; field of view = 192×192

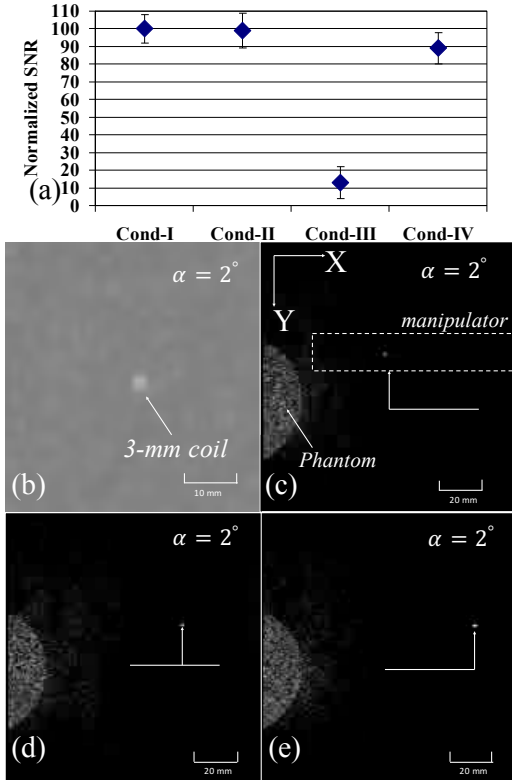


Fig. 8. (a) shows the SNR for four conditions relative to baseline, (b) shows an image of the marker while the motor was actuated zoomed and windowed, (c) - (d) show frames during the actuation of the manipulator

mm<sup>2</sup>; slice thickness = 10 mm).

In the first study, images were collected for two conditions: (i) baseline of the phantom, with no hardware in place and (ii) the 1-DoF secured over the phantom, the SMT tubing filled with media, but no electronics or servo motor in the room. As expected from the use of MR inert material, no difference was observed between the two conditions. In the second study,  $n = 20$  images were collected for each one of the conditions; (I) baseline with hardware unpowered, (II) electronics powered and motor idle, (III) motor running, i.e. manipulator actuated, without filtering, (IV) motor running with filtering. Images were analyzed to calculate the signal-to-noise Ratio (SNR), i.e. the ratio of the signal from a region-of-interest (ROI) in the phantom to the standard deviation of the signal on an ROI placed in empty space. SNR values were normalized to the mean at condition (I) and reported as the average standard deviation. Fig. 8a shows the SNR for the four conditions illustrating that, relative to baseline (Condition I), (a) in Condition II, the SNR was  $99 \pm 9\%$ , (b) in Condition III, the SNR was  $13 \pm 8\%$ , and (c) in Condition IV, the SNR is  $89 \pm 9\%$ . Filtering combined with shielding and grounding of the Faraday cage recovered the SNR with losses of 11% of the baseline. This is in accord with prior studies that used electromagnetic motors [23] and [34]. The third study assessed tracking the SMT-actuated manipulator with an MR marker made of a 3-mm diameter solenoid small inductively-coupled RF coil that surrounded a

Table 1: Review and Conclusions of Modeling and Experiments

Theoretical / Modeling:
<ul style="list-style-type: none"> <li>• Friction increases with length <math>L_{SMT}</math> of conduit.</li> <li>• Friction is reduced by increasing spacer <math>L_{spacer}</math>.</li> <li>• Max. bend is limited by spacer dimensions (<math>L_{spacer}</math> and <math>D_{spacer}</math>).</li> </ul>
Experimental Studies:
<ul style="list-style-type: none"> <li>• Closed-loop position control error can reach <math>0.075 \pm 0.042</math> mm accuracy.</li> <li>• Exceptionally long response times due to:               <ul style="list-style-type: none"> <li>(i) inefficient packing and (ii) PID controller.</li> </ul> </li> <li>• Electromagnetic motor can be used inside the MR scanner room with shielding and filtering.</li> </ul>
Conclusions / Future Directions:
<ul style="list-style-type: none"> <li>• Convert to low friction coefficient material (e.g. PTFE with <math>\mu = 0.04</math> vs <math>\mu = 0.25</math> for nylon).</li> <li>• Maintain high length and adjust diameter of spacers per desired bending as in Equation (4).</li> <li>• Implement improved packing: (a) extendable mechanism and/or (b) two motors arranged antagonistically, each actuating in different directions.</li> </ul>

source of MR signal. The marker was attached to the actuated stage of the 1-DoF SMT-actuated manipulator then secured between two homogeneous phantoms onto the patient couch. The manipulator was then actuated to move back and forth between two end positions while images were collected with the same TrueFISP as above, but with a very small excitation angle of  $2^\circ$  needed for operation of inductively coupled coils. Fig. 8b shows an image of the marker while the motor was actuated zoomed and windowed to appreciate the noise level, demonstrating that the operation of the motor did not affect imaging, even with the very small angle that is more prone to EMI. Fig. 8c to e show frames during the actuation of the manipulator (delineated with the dashed white box) depicting the marker coil signal at three locations (white arrows). These studies demonstrated that an SMT-actuated manipulator could be tracked during servo-motor actuation with inductively coupled coils. This is one method a device could be tracked during MR-guided procedures.

#### IV. DISCUSSION

SMT was originally introduced as an alternative force transmission mechanism which is functionally comparable to hydraulic or pneumatic systems. As experience is accumulated from simulation and experimental studies we can conclude that SMT may be a viable option because it is stable, repeatable, offers higher stiffness than fluidics, and can achieve high precision. However SMT, in the implementation for these studies, exhibited major limitations originating from friction and tubing deformation. In the following sections we discuss our findings and review them in Table 1. The lower row of Table 1 provides a list of aspects that must be taken into account in future works.

##### A. Friction

Friction is the single most important factor that affects SMT operation. As shown as Fig. 3, the most obvious and direct solution is to use low coefficient-of-friction materials. In response, we plan to change the nylon tubing and nylon

spheres to Polytetrafluoroethylene (PTFE) lined tubing and PTFE spheres. This will reduce the coefficient of friction  $\mu$  from 0.25 (nylon-to-nylon) to 0.04 (PTFE-to-PTFE). Based on the above simulations, we expect that this may dramatically improve the force transmission efficiency as well as the closed loop control. This change is complicated by the challenge of ensuring that the PTFE tubing will not expand resulting in elasticity and non-linearities.

### B. Experimental set-up

Expansion is the main problem in the fluidic system; the stiffness of SMT is much higher than a hydraulic or pneumatic system. However, the Nylon sphere and inner tube experience deformation. To minimize this, in future studies we will explore alternate materials. We plan to change sphere materials from nylon to glass or Delrin. There is a nearly 1-millimeter clearance between an acrylic conduit and inner tube. As we mentioned, we plan to change to PTFE inner tube. We also plan to use a braided hose, in which the cover is Kevlar, a MR compatible, nonconductive and nonmagnetic material, and the inner tube is made of PTFE. The current set-up does not measure preload. Our experimental protocol begins with preloading the SMT. The application of preload has a trade-off: high preload force eliminates gaps, but stretches the nylon tubing, while low force may not remove all gaps. Future work will use an antagonistic pair of motors for each SMT DoF, so that preload pressure can be controlled in each direction. In the experiment, we preloaded the whole SMT line by manually filling spheres. It could reduce but not eliminate backlash. Effects from backlash appear in system error and delay. Thus, we need to design a new mechanism to overcome this disadvantage. We will design a new motor base, which motor can slide and fix on, to complete the preload process.

### C. MR Compatibility of SMT

As expected from the use of nonconductive and nonmagnetic SMT componentry (nylon) and manipulator material (Delrin), studies validated that they are MR safe (i. e., pose no known hazards in all MR environments and conditions as defined in [35]). In this work, the SMT lines were powered by conventional electromagnetic motors. While these motors are considered non-MR compatible, they are used in the MR room: e.g., servomotors on MR patient couches, the FDA-cleared MRI-radiation therapy system with 180 DC servomotors (ViewRay [36]), a valve phantom [37], and our cardiac phantom with 18 electromagnetic stepper motors [34]. Placing the motor and electronics well outside the 5 Gauss line of the scanner and using low-pass filtering and grounded Faraday shielding of the components reduced EMI (filtered SNR 89% vs. unfiltered SNR 13% of control). Those data validated our observations from prior studies with stepper motors [23], [34]. Electromagnetic motors were selected since they offer high off-the-shelf availability, low cost, high torque and experience in the engineering community. Due to specific positioning (away from the 5G line) and the filtering and shielding of the control unit the system is MR

Conditional (i.e. the item has been demonstrated to pose no known hazards with a specified conditions of use, as defined in [35]). Whether such motors will be used in studies on humans must be determined with extensive studies.

## V. CONCLUSION AND FUTURE WORK

MR compatible manipulators are a main theme in the field of interventional MRI, and pioneering groundbreaking works have advanced this concept to reality. Efforts are continuing toward new actuation and robot designs for eventual clinical use. SMT was introduced as a simple and low-cost transmission exhibiting certain features similar to fluidic systems for MR manipulation: conduit routing and remote transfer of actuation. The data presented herein illustrated that closed-loop SMT can achieve sub-millimeter accuracy yet underscored the main limitations that need to be addressed: friction and media packing to ensure the SMT backbone performs as theoretically expected. The presented studies had certain limitations. First, benchtop studies were limited to 1 meter long SMT tubing. While they resulted in a valuable understanding of the mechanism, after implementation of a low-friction SMT version we plan to systematically characterize SMT performance. It is noted that MR studies were performed with 4-meter long SMT lines but with open-loop control because effect on MR images was the subject, not control. Second, the choice of material was not optimal. Nylon tubing and spheres have a coefficient of friction of 0.25, while PTFE-to-PTFE is 0.04. Those studies underscored the importance of material considerations affecting the elasticity of the system. Third, manual media packing was not optimal causing small gaps in the SMT backbone. Friction, suboptimal media packing and tube elasticity may have contributed to the nonlinearity of the system and the long rise time during closed-loop control. A mechanism to establish and maintain media packing is under development. In this work, MRI studies employed servo motors inside the MR scanner room by placing them outside the 5 Gauss line and using filtering and shielding to reduce EMI. Additional studies are needed to further characterize the conditions for their use, as well as further improve EMI reduction. SMT is a new mechanism, and there is limited data about its operation. Further studies are needed to investigate and optimize material and dimensions of componentry, control laws, SMT-specific manipulators, and mechanism, to explore this transmission for actuating manipulators.

## ACKNOWLEDGMENT

This work was supported by the National Science Foundation Grants CNS-0932272 and IIP-1622946. All opinions and conclusions or recommendations expressed in this work reflect the views of authors not our sponsors.

## REFERENCES

- [1] N. V. Tsekos, A. Khanicheh, E. Christoforou, and C. Mavroidis, "Magnetic resonance-compatible robotic and mechatronics systems for image-guided interventions and rehabilitation: a review study," *Annu. Rev. Biomed. Eng.*, vol. 9, pp. 351–387, 2007.

- [2] T. Fisher, A. Hamed, P. Vartholomeos, K. Masamune, G. Tang, H. Ren, and Z. T. Tse, "Intraoperative magnetic resonance imaging—conditional robotic devices for therapy and diagnosis," *Proceedings of the Institution of Mechanical Engineers, Part H: Journal of Engineering in Medicine*, vol. 228, no. 3, pp. 303–318, 2014.
- [3] P. Mozer, J. Troccaz, and D. Stoianovici, "Urologic robots and future directions," *Current opinion in urology*, vol. 19, no. 1, p. 114, 2009.
- [4] M. Moche, D. Zajonz, T. Kahn, and H. Busse, "MRI-guided procedures in various regions of the body using a robotic assistance system in a closed-bore scanner: Preliminary clinical experience and limitations," *Journal of Magnetic Resonance Imaging*, vol. 31, no. 4, pp. 964–974, 2010.
- [5] M. M. Arnolli, N. C. Hanumara, M. Franken, D. M. Brouwer, and I. A. Broeders, "An overview of systems for CT-and MRI-guided percutaneous needle placement in the thorax and abdomen," *The International Journal of Medical Robotics and Computer Assisted Surgery*, vol. 11, no. 4, pp. 458–475, 2015.
- [6] G. S. Fischer, A. Krieger, I. Iordachita, C. Csoma, L. L. Whitcomb, and G. Fichtinger, "MRI compatibility of robot actuation techniques—a comparative study," in *International Conference on Medical Image Computing and Computer-Assisted Intervention*. Springer, 2008, pp. 509–517.
- [7] N. V. Tsekos, E. Yacoub, P. V. Tsekos, and I. G. Koutlas, "Design of an MRI-compatible robotic stereotactic device for minimally invasive interventions in the breast," *J. Biomechanical Eng.*, vol. 126, no. 4, pp. 458–465, 2004.
- [8] G. Li, H. Su, G. A. Cole, W. Shang, K. Harrington, A. Camilo, J. G. Pilitsis, and G. S. Fischer, "Robotic system for MRI-guided stereotactic neurosurgery," *IEEE Transactions on Biomedical Engineering*, vol. 62, no. 4, pp. 1077–1088, 2015.
- [9] N. V. Tsekos, A. Özcan, and E. Christoforou, "A prototype manipulator for magnetic resonance-guided interventions inside standard cylindrical magnetic resonance imaging scanners," *Journal of biomechanical engineering*, vol. 127, no. 6, pp. 972–980, 2005.
- [10] A. Krieger, I. Iordachita, S.-E. Song, N. B. Cho, P. Guion, G. Fichtinger, and L. L. Whitcomb, "Development and preliminary evaluation of an actuated MRI-compatible robotic device for MRI-guided prostate intervention," in *Robotics and Automation (ICRA), 2010 IEEE International Conference on*. IEEE, 2010, pp. 1066–1073.
- [11] M. Muntener, A. Patriciu, D. Petrisor, D. Mazilu, H. Bagga, L. Kavoussi, K. Cleary, and D. Stoianovici, "Magnetic resonance imaging compatible robotic system for fully automated brachytherapy seed placement," *Urology*, vol. 68, no. 6, pp. 1313–1317, 2006.
- [12] S.-E. Song, N. B. Cho, G. Fischer, N. Hata, C. Tempany, G. Fichtinger, and I. Iordachita, "Development of a pneumatic robot for MRI-guided transperineal prostate biopsy and brachytherapy: New approaches," in *Robotics and Automation (ICRA), 2010 IEEE International Conference on*. IEEE, 2010, pp. 2580–2585.
- [13] A. Kapoor, B. Wood, D. Mazilu, K. A. Horvath, and M. Li, "MRI-compatible hands-on cooperative control of a pneumatically actuated robot," in *Robotics and Automation, 2009. ICRA'09. IEEE International Conference on*. IEEE, 2009, pp. 2681–2686.
- [14] M. Li, A. Kapoor, D. Mazilu, and K. A. Horvath, "Pneumatic actuated robotic assistant system for aortic valve replacement under MRI guidance," *IEEE Transactions on Biomedical Engineering*, vol. 58, no. 2, pp. 443–451, 2011.
- [15] G. Ganesh, R. Gassert, E. Burdet, and H. Bleuler, "Dynamics and control of an MRI compatible master-slave system with hydrostatic transmission," in *Robotics and Automation, 2004. Proceedings. ICRA'04. 2004 IEEE International Conference on*, vol. 2. IEEE, 2004, pp. 1288–1294.
- [16] R. Gassert, R. Moser, E. Burdet, and H. Bleuler, "MRI/fMRI-compatible robotic system with force feedback for interaction with human motion," *IEEE/ASME transactions on mechatronics*, vol. 11, no. 2, pp. 216–224, 2006.
- [17] D. Stoianovici, A. Patriciu, D. Petrisor, D. Mazilu, and L. Kavoussi, "A new type of motor: pneumatic step motor," *IEEE/ASME Transactions On Mechatronics*, vol. 12, no. 1, pp. 98–106, 2007.
- [18] E. G. Christoforou, A. Ozcan, and N. V. Tsekos, "Robotic arm for magnetic resonance imaging guided interventions," in *Biomedical Robotics and Biomechanics, 2006. BioRob 2006. The First IEEE/RAS-EMBS International Conference on*. IEEE, 2006, pp. 911–916.
- [19] A. A. Goldenberg, J. Trachtenberg, W. Kucharczyk, Y. Yi, M. Haider, L. Ma, R. Weersink, and C. Raoufi, "Robotic system for closed-bore MRI-guided prostatic interventions," *IEEE/ASME Transactions On Mechatronics*, vol. 13, no. 3, pp. 374–379, 2008.
- [20] G. S. Fischer, G. Cole, and H. Su, "Approaches to creating and controlling motion in MRI," in *Engineering in Medicine and Biology Society, EMBC, 2011 Annual International Conference of the IEEE. IEEE*, 2011, pp. 6687–6690.
- [21] A. E. Sonmez, A. G. Webb, W. M. Spees, A. Ozcan, and N. V. Tsekos, "A system for endoscopic mechanically scanned localized proton MR and light-induced fluorescence emission spectroscopies," *Journal of Magnetic Resonance*, vol. 222, pp. 16–25, 2012.
- [22] N. Yu, C. Hollnagel, A. Blickenstorfer, S. S. Kollias, and R. Riener, "Comparison of MRI-compatible mechatronic systems with hydrodynamic and pneumatic actuation," *IEEE/ASME transactions on mechatronics*, vol. 13, no. 3, pp. 268–277, 2008.
- [23] X. Liu, D. Biediger, R. Kopru, E. G. Christoforou, and N. V. Tsekos, "A new transmission mechanism for the actuation of manipulators for magnetic resonance imaging (MRI) guided interventions," in *XIV Mediterranean Conference on Medical and Biological Engineering and Computing 2016*. Springer, 2016, pp. 673–678.
- [24] L. Huang, X. Liu, N. V. Tsekos, and A. T. Becker, "Two missing components for solid media transmission: Amplifiers and manifolds," in *Automation Science and Engineering (CASE), 2016 IEEE International Conference on*. IEEE, 2016, pp. 207–212.
- [25] H. Zhao and A. T. Becker, "BlockPushingIROS2015, <https://github.com/roboticswarmcontrol/smt1m1dofpaper/code>," Mar. 2017.
- [26] L. Xin, H. Li, B. A. T. H. M. J., and T. N. V., "Open-loop control studies of a solid-media transmission actuator," 2016, submitted.
- [27] V. Agrawal, W. J. Peine, and B. Yao, "Modeling of transmission characteristics across a cable-conduit system," *IEEE Transactions on Robotics*, vol. 26, no. 5, pp. 914–924, 2010.
- [28] K. J. Åström and B. Wittenmark, *Computer-controlled systems: theory and design*. Courier Corporation, 2013.
- [29] R. Dhaouadi, K. Kubo, and M. Tobise, "Two-degree-of-freedom robust speed controller for high-performance rolling mill drives," *IEEE transactions on industry applications*, vol. 29, no. 5, pp. 919–926, 1993.
- [30] M. Nordin and P.-O. Gutman, "Controlling mechanical systems with backlash, a survey," *Automatica*, vol. 38, no. 10, pp. 1633–1649, 2002.
- [31] J. Tal, "General dual loop improves backlash compensation," *ServoTrends*, vol. 14, no. 4, pp. 3–4, 1998.
- [32] H. Garnier, M. Mensler, and A. Richard, "Continuous-time model identification from sampled data: implementation issues and performance evaluation," *International Journal of Control*, vol. 76, no. 13, pp. 1337–1357, 2003.
- [33] L. Ljung, "Experiments with identification of continuous time models," *IFAC Proceedings Volumes*, vol. 42, no. 10, pp. 1175–1180, 2009.
- [34] N. C. von Sternberg, Y. S. Hedayati, H. M. Zaid, E. Yenziaras, E. Christoforou, and N. V. Tsekos, "An actuated phantom for developing and studying MRI-guided interventions in dynamic environments," in *Biomedical Robotics and Biomechanics (BioRob), 2012 4th IEEE RAS & EMBS International Conference on*. IEEE, 2012, pp. 1669–1674.
- [35] *Standard Practice for Marking Medical Devices and Other Items for Safety in the Magnetic Resonance Environment*, American Society for Testing and Materials International, West Conshohocken, PA, 2003.
- [36] "Three multileaf collimators," <http://www.maxonmotorusa.com/maxon/view/content/application/viewray>.
- [37] M. S. Jackson, S. R. Igo, T. E. Lindsey, D. Maragiannis, K. E. Chin, K. Autry, R. Schutt III, D. J. Shah, P. Valsecchi, W. B. Kline *et al.*, "Development of a multi-modality compatible flow loop system for the functional assessment of mitral valve prostheses," *Cardiovascular Engineering and Technology*, vol. 5, no. 1, pp. 13–24, 2014.